Environmental Science and Pollution Research (2022) 29:82297–82308
https://doi.org/10.1007/s11356-022-21633-9

RESEARCH ARTICLE

Construction of WO_3 nanocubes@Loess for rapid photocatalytic degradation of organics in wastewater under sunlight

Hua Yang[1] · Peiyu Cao[1] · Yaping Zhang[1] · Meiling Zhou[1] · Qianqian Wang[1] · Rongmin Wang[1] · Pengfei Song[1] · Yufeng He[1]

Received: 29 March 2022 / Accepted: 19 June 2022 / Published online: 25 June 2022

Abstract

In nowadays, environmental pollution has been greatly improved, but the development of low-cost and environmentally friendly materials are still challenge in the field of water treatment. Herein, a cheap and eco-friendly natural loess particle (LoP) was used for in situ growth of tungsten trioxide nanocubes (WO_3NCs) on its surface via a simple one-pot hydrothermal method, which afforded a stable loess-based photocatalyst (WO_3NCs@LoP). It was characterized by scanning electron microscopy (SEM), X-ray diffraction (XRD), Fourier transform infrared spectroscopy (FT-IR) analysis, UV–Vis diffuse reflectance spectra (UV–Vis DRS), and X-ray photoelectron spectroscopy (XPS). The photocatalytic performances of WO_3NCs@LoP were applied to photodegradation of organics under visible-light illumination. It was found that the removal rate of methylene blue (MB) got to 99% within 20 min, which was higher than that of materials, such as pure LoP and WO_3NCs. Moreover, the photocatalytic activity of WO_3NCs@LoP remained 85% after 9 cycling times, indicating its high stability and reusability. It was suggested that the synergy of the well narrowed band gap and effectual control of e^--h^+ recombination in WO_3NCs@LoP improve its photodegradation efficiency. In summary, using natural minerals (LoP) as carrier, a novel eco-friendly photocatalyst could be explored for photodegradation of organic pollutions in wastewater treatment.

Keywords WO_3 nanocubes@Loess · Loess-based photocatalyst · Eco-friendly carrier · Photodegradation · Synergistic effect · Mechanism

Introduction

With the acceleration of urbanization, the rapid development of industry and climate change of many rivers as well as lakes had been badly polluted, especially in developing countries, which directly affect the healthy drinking water of human beings (Mirzaeian et al. 2019; Gupta et al. 2015; Cheng and Jin 2022; Shi et al. 2022; Liu et al. 2021). Numerous organic pollutants have been identified in various sources of wastewater (Malinga and Jarvis 2020; Kamaludin et al. 2018; Masocha et al. 2022). For example, Ahmadi et al. reported the ZnO@ZIF-67 nanocomposite with high adsorption performance for the removal of pharmaceutical contaminant from aqueous media (Ahmadi et al. 2021, 2022). In recent years, the dyes can cause the decrease of water transmittance and hinder the growth of bacteria and other micro-organisms, inhibiting the aquatic photosynthesis and damage the ecosystem; at the same time, dyes are harmful to human beings (Robati et al. 2016; Rajabi et al. 2017). Cationic dyes methylene blue is widely used as colorants in industry and bacteriostatic agents. Researchers found that these azo dyes are carcinogenic, highly toxic, persistent, and mutagenic; it caused irretrievable damage to the environment if it discharged into water (Rajabi et al. 2019; Abdelmaksoud et al. 2021). It was reported that adsorption process is one of the effective methods to remove dyes and antibiotics from wastewaters (Moradi and Sharma 2021). The polymer, such as carboxylmethyl cellulose and guar gam, were composited with graphene oxide, Fe_3O_4 or TiO_2, and the obtained

Responsible Editor: Sami Rtimi

Hua Yang and Peiyu Cao are the co-first author.

✉ Yufeng He
heyufeng@nwnu.edu.cn

[1] Key Lab. Eco-Functional Polymer Materials of MOE, Institute of Polymer, College of Chemistry & Chemical Engineering, Northwest Normal University, Lanzhou 730070, China

composite adsorbents were used for removal of anionic and cationic dyes, such as methylene blue (MB), methyl orange (MO), and malachite green (MG), from aqueous solution (Naeini et al. 2022; Moradi et al. 2021). In past decades, some systems, including physical, chemical, and biological processes, were explored to treat contaminated water and improve effluent water quality (Rajendran et al. 2021; Moradi et al. 2009; Truong et al. 2022; Dhanalakshmi et al. 2020; Li et al. 2019), but there are still a lot of questions. Therefore, finding an efficient and economical approach to remove and degrade multiple pollutants from water is extremely critical (Babaei et al. 2022; Shi et al. 2020; Liu et al. 2019).

Since the discovery of semiconductor heterogeneous photocatalysis, it has become a potential solution for degrading toxic organic pollutants to achieve environmental sustainability (Mukhtar et al. 2021). And semiconductive photocatalyts have shown excellent development prospects in the field of industrial wastewater and domestic wastewater treatment (Ouyang et al. 2021; Chen et al. 2020). Tungsten trioxide (WO_3) is an n-type semiconductor that has been vastly studied for applications in gas sensing, catalysis, solar energy conversion, and electrochromic displays (Lu et al. 2022). The low energy band gap of WO_3 allows this material a very promising candidate for the green energy production to implement the world energy demand (Naeimi et al. 2022; Tahir et al. 2018). Layered WO_3 nanocubes could inhibit the recombination of photoelectron-hole pairs (Parthibavarman et al. 2018), thereby enhancing the redox properties of nanoparticles, which has attracted much attention in the field of electrochemical and photocatalytic materials (Mehmood et al. 2018). However, in the semiconductor of nubbly WO_3, the surface accumulation of photogenerated charge carriers was easy, which lead to increase their recombination rate and eventually tumbling the photocatalytic efficiency (Manikandan et al. 2022; Shah et al. 2020; Sun et al. 2020). To settle these problems, numerous effective efforts, such as construction of heterojunction (Sun et al. 2022), modification (Karami et al. 2022), metal doping (Raeisi et al. 2021; Al-Kuhailia and Drmoshb 2022), and quantum dot modification (Cui et al. 2020) which strengthen the separation of photocarrier and improve photocatalytic performance, have been researched. For improving the recyclability and performance of photocatalysts, natural non-metallic minerals were used as carriers to disperse the photocatalysts (Li et al. 2022; Shen et al. 2021). The loess is mainly composed of extremely small powdery particle. It has high hydrophilicity and pores of various sizes and shapes, so that the loess has certain adsorption properties (Babudurai et al. 2021; Xu et al. 2022; Gao et al. 2021). With the increasing shortage of non-renewable resources, the construction of WO_3 nanocubes@Loess has good prospects for rapid photocatalytic degradation of organics in wastewater.

In order to enhance the photocatalytic performance of WO_3-based compounds, in this paper, the particles of LoP, a kind of extremely common and inexpensive natural silicate particles with metastable structure, were used as inorganic carrier; the WO_3NCs was attached by in situ deposition, which afforded WO_3NCs@LoP. After being characterized by SEM, XRD, FT-IR, XPS analysis, and UV–Vis DRS. In addition, its photocatalytic performance was investigated by photocatalytic degradation of dyes under visible light, and its synergistically photocatalytic performance was investigated.

Experimental

Materials

Loess was collected from the local hill near Lanzhou of China. Sodium tungstate dihydrate ($Na_2WO_4{\cdot}2H_2O$) used in the experiments was purchased by second branch of Shanghai Reagent General Plant. Citric acid monohydrate ($C_6H_8O_7{\cdot}H_2O$, CA) was obtained by Tianjin Deen Chemical Reagent Co. Ltd. Anhydrous ethanol (C_2H_6O) was purchased by Sinopharm chemical Reagent Co. Ltd. Hydrochloric acid (HCl, Shanghai Zhongqin Chemical Reagent Co. Ltd.). Other reagents, such as isopropanol (IPA) (Tianjin Fuchen Chemical Reagent Factory), disodium ethylenediaminetetraacetate (EDTA-2Na) (Sinopharm Chemical Reagent Co. Ltd.), silver nitrate ($AgNO_3$, Third Branch of Tianjin Chemical Reagent Sixth Factory), rhodamine B (RhB, Tianjin Tianxin Fine Chemical Development Center), methylene blue trihydrate (MB), malachite green (MG), crystal violet (CV), and Eriochrome Black T (EBT) were purchased from Sinopharm Chemical Reagent Co. Ltd.. All the above chemicals were of analytical grade and directly used without further purification. The redistilled water was used during the experiment procedures.

Separation of loess particles (LoP)

100 g of dried loess powder was dispersed in water and stirred for 12 h with mechanical at room temperature until loess particles being dispersed completely. Firstly, the supernatant suspension was quickly collected after 2 min standing of the loess powder turbid solution. Secondly, the obtained 300 mL of supernatant suspension was stirred for 20 min. Then, after standing for 10 min, the supernatant suspension was collected. Thirdly, the above 200 mL of supernatant suspension stood for 24 h, the clear water layer was sucked out. The small loess particles (LoP) were obtained by drying 12 h.

Preparation of WO_3NCs@LoP

WO_3NCs@LoP composite materials were prepared by hydrothermal method; the process was as follows: 1.0 g of $Na_2WO_4{\cdot}2H_2O$ powder and 0.5 g of CA were dispersed into 50 mL of deionized water, and then 10 mL of 4 mol•L^{-1} HCl was added dropwise. Then amounts of LoP were uniformly dispersed in the mixed solution, and the mixed solution was transferred to a 100-mL Teflon-lined stainless-steel autoclave and heated at 160 °C for 12 h. The light-yellow solid powder products were obtained by centrifugation and then washed with deionized water followed by ethanol for 3–5 times. Finally, a square WO_3NCs@LoP photocatalyst was obtained at 60 °C by vacuum drying for 4 h. The WO_3NCs@LoP-1, the WO_3NCs@LoP-3, the WO_3NCs@LoP-7, and the WO_3NCs@LoP-9 samples were prepared via adjusting the amount of LoP, and the rest of steps was the same. The obtained photocatalysts were marked as WO_3NCs@LoP-x (x = 1, 3, 5, 7, 9 denoted the mass of LoP). For comparison, pure WO_3NCs was prepared without introducing LoP by using the same method.

Characterization

The mineralogical composition and crystalline phase structure were measured by X-ray diffraction (XRD) using Cu Ką radiation at 40 kV, 40 mA, and a step size of 0.02° in the range of 5 ~ 80°. FT-IR spectra were recorded between 4000 and 400 cm^{-1} through the KBr method with the FTS-3000 spectrophotometer. The morphology and particle size were observed by scanning electron microscope (SEM) (at 5 kV, ULTRA Plus microscope, Germany). UV–Vis diffuse reflectance spectra (UV–Vis DRS) were collected on a UV-2800A spectrophotometer in the range of 200–800 nm. The average particle size was measured by dynamic light scattering (DLS) (Nano Series, Malvern Instruments Ltd., UK). The elemental composition and chemical oxidation state of the sample were analyzed with X-ray photoelectron spectroscopy (XPS, Thermo Scientific K-Alpha).

Photocatalytic reaction

The photocatalytic activity of the composite was evaluated by measuring the degradation rates of MB in synthetic wastewater (Fig S1). In addition to the organic dyes MB, which were used as model pollutants, the synthetic wastewater mostly contains inorganic NaCl, Na_2CO_3, and NaH_2PO_4. And A 500 W Xe lamp with cut-off filter (λ > 420 nm) was served as light source to simulate sunlight. A set of photocatalytic degradation experiments were performed with the following procedure: 0.05 g WO_3NCs@LoP was added to 50 mL of MB solution (20 mg•L^{-1}). The adsorption–desorption equilibrium of MB was established after stirring in the dark for 30 min and then degraded MB under light. At set intervals, the samples were withdrawn from the reactor and filtered by PES syringe filter (pore size: 0.22 μm) for removal of photocatalyst particles. Finally, the UV spectrophotometer was used to determine the absorbance of the solution at 664 nm. All photocatalytic experiments were repeated at least three times, and error bars were calculated. The degradation efficiency of the catalyst was determined by using Eq. 1.

$$\eta = \left[\left(C_O - C_t\right)/C_0\right] \times 100\% \quad (1)$$

where C_0 is the initial concentration of the dye solution and C_t is the concentration MB after photocatalytic degradation for certain reaction time.

Capture of radical experiment

In the photocatalytic process, the active substances produced in the degradation process were captured by adding a trapping agent (1 mmol/L), where $AgNO_3$ (1 mmol/L), benzoquinone (BQ, 1 mmol/L) isopropyl alcohol (IPA, 1 mmol/L), and EDTA-2Na (1 mmol/L) were viewed as the capture of e^-, •O^{2-}, •OH, and h^+ species, respectively. Except the addition of trapping agent in the experimental process, other operations and conditions kept consistent with the photocatalytic process.

Results and discussion

Preparation and characterization of WO_3NCs@LoP

The preparation process WO_3NCs@LoP was shown in Scheme 1. Using LoP, a kind of extremely common and inexpensive natural silicate particles with metastable structure, as inorganic carrier, the WO_3NCs loaded on loess particles in situ depositing, WO_3NCs@LoP. The photocatalytic degradation process is the result of the synergistic effect of adsorption and degradation (Cao et al. 2022). Although WO_3NCs has a certain extent photocatalytic activity, its adsorption performance is relatively poor. Dual-functional environmentally friendly composite photocatalyst was prepared by using the adsorption property of loose loess particles and synergistically with the photocatalytic properties of WO_3NCs, which was favorable for enhancing the photocatalytic activity. It is of great guiding significance to construct environmentally friendly photocatalysts.

The photocatalytic properties of the WO_3NCs@LoP were studied by photocatalytic degradation of MB, which were exhibited in Table S1, pure hexagonal-WO_3 nanocubes only 66.11% degradation rate of MB. Varying the ratio of the WO_3NCs@LoP by adjusting the amount of LoP and

Scheme 1 Formation of WO_3NCs@LoP photocatalyst

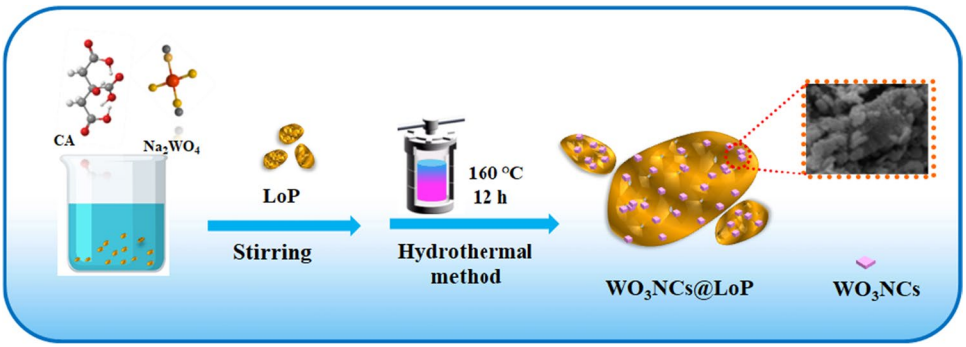

photocatalytic performance for degradation of MB under visible light irradiation was compared. It could be observed that WO_3NCs@LoP expressed the best photocatalytic performance (the amount of loess added was 5 g, 99.77%). Therefore, this WO_3NCs@LoP was characterized and discussed in detail.

SEM analysis

The micromorphology of WO_3NCs@LoP and its materials (LoP, WO_3NCs) were observed by SEM, and the results were shown in Fig. 1. LoP were irregular particles with cracks with relatively loose structure (Fig. 1a), which was beneficial to exposing large surface area. The morphology of WO_3NCs looked like nanocubes with smooth surface, and the average size was near 100 nm (Fig. 1b). But it was easy to agglomerate as reported results (Dhanalakshmi et al. 2020; Manikandan et al. 2022 and Palanisamy et al. 2021). In WO_3NCs@LoP (Fig. 1c), the nanocubes of WO_3NCs were tightly attached to LoP, which was well-dispersed on surface of the particles for avoiding agglomeration. The particle size of WO_3NCs@LoP was measured by DLS. It showed that the average size of composites was near 780 nm (Fig. S2), which was similar to SEM results.

FT-IR analysis

The FT-IR spectra of LoP, WO_3NCs, and WO_3NCs@LoP were shown in Fig. 2. In WO_3NCs, the characteristic peak near 800 ~ 645 cm^{-1} was attributed to the vibration of the W–O-W bond (Manikandan et al. 2022). The characteristic peaks of LoP appeared at 1084 cm^{-1} and 490 cm^{-1} (Deng et al. 2022), which were attributed to the stretching and bending vibration peaks of Si–O-Si in LoP. The wide peak at 3600 ~ 3300 cm^{-1} was related to the stretching vibration absorption peak of hydroxyl (-OH) in water. Comparing with pure LoP and WO_3NCs, their characteristic peaks appeared in WO_3NCs@LoP. It shows that WO_3NCs is successfully loaded on the surface of loess, and the structure is extremely stable, which is consistent with the SEM results.

Fig. 1 The SEM images of LoP (**a**), WO_3NCs (**b**), and WO_3NCs@LoP (**c**)

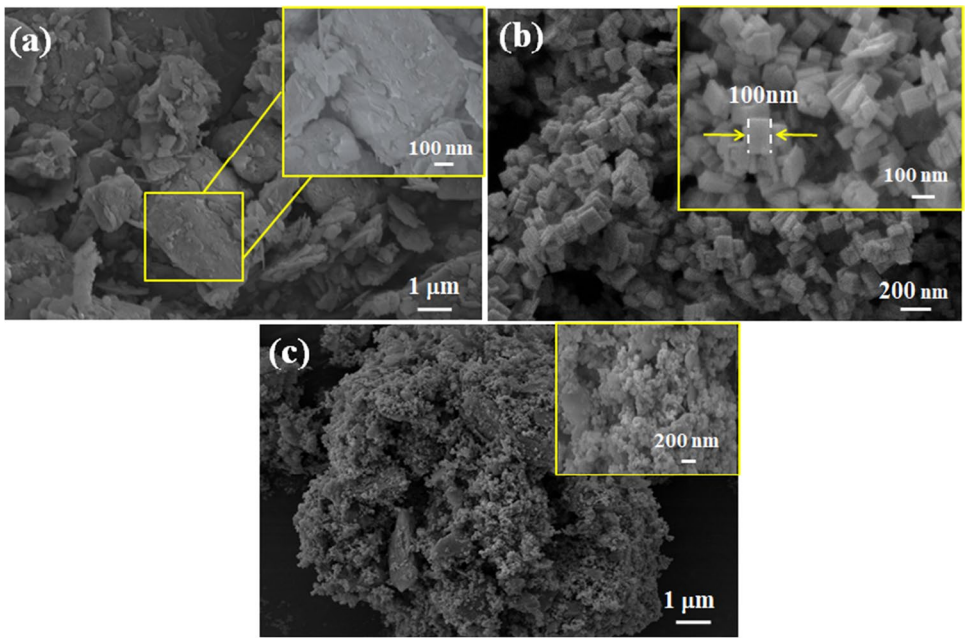

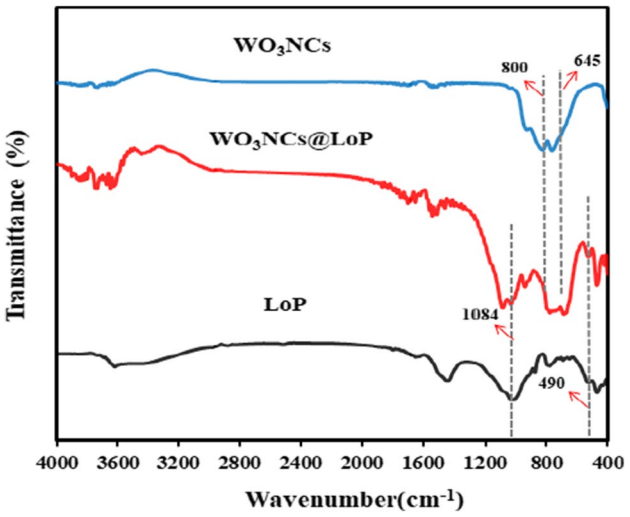

Fig. 2 The FT-IR spectra of LoP, WO_3NCs, and WO_3NCs@LoP

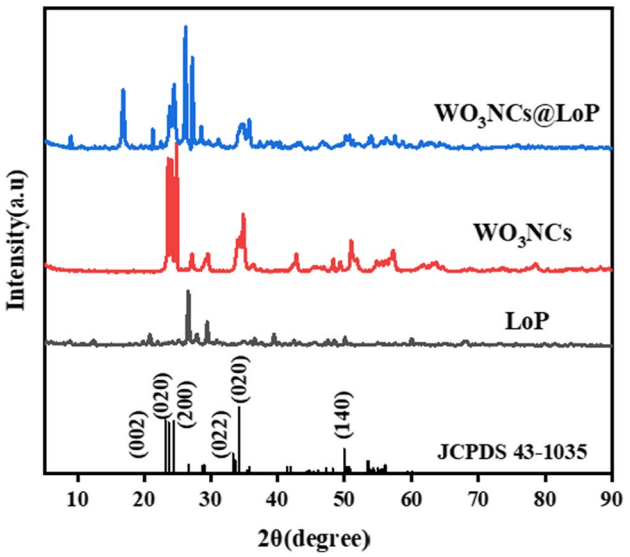

Fig. 3 The XRD diagram of LoP, WO_3NCs, and WO_3NCs@LoP

XRD analysis

The X-ray diffraction (XRD) was used to investigate the crystalline structure, and the results were shown in Fig. 3. For the WO_3NCs XRD pattern, some peaks at 23.1°, 23.5°, 24.4°, 33.2°, 33.6°, 34.1° and 49.9° indexed to the (002), (020), (200), (022), (−202), (202), and (140) planes, which was consistent with WO_3NCs standard XRD patterns (JCPDS card no: 43–1035) (Zhang et al. 2021; Guo et al. 2019), proving that the material was successfully synthesized. The LoP XRD pattern could be seen; the diffraction peak at 28°, 26°, 50°, 60°, and 68° were the characteristic diffraction peak of amorphous silicate or aluminosilicate and quartz in LoP. The characteristic peaks of WO_3NCs and LoP were appeared in WO_3NCs@LoP, indicating that WO_3NCs@LoP was successfully synthesized, and the crystal structure was not destroyed during the synthesis process, which was mutually confirmed with SEM and FT-IR.

XPS analysis

In order to illustrate the chemical composition and valence structure, WO_3NCs@LoP and LoP were analyzed by XPS spectroscopy, and the results were shown in Fig. 4. In the XPS survey spectrum of WO_3NCs@LoP (Fig. 4a), W was clearly appeared besides some typical elements of LoP, such as Si, Al, O, Fe, K, and C. The distribution of these elements was summarized in Table S2. In the XPS survey spectrum of LoP (Fig. 4b), W was not found. In the W4f high resolution spectrum (Fig. 4a1), it exhibited two typical peaks around 35.7 and 37.8 eV which were assigned to the $W4f_{7/2}$ and $W4f_{5/2}$ for W^{6+} oxidation states in WO_3NCs@LoP composite, respectively (Dhanalakshmi et al. 2020), whereas the characteristic peaks of W4f element cannot be observed in the bare LoP (Fig. 4b1). It further proved the successful synthesis of composite materials. Besides, for Si2p as shown in Fig. 4a2, the peak value at 103.0 eV belonged to SiO_2 (Ye et al. 2022), which was similar to LoP (Fig. 4b2), indicating the stability of the material. The result was consistent with FT-IR, SEM, and XRD, confirming that the WO_3NCs@LoP was successfully synthesized.

In summary, based on SEM, XRD, FT-IR, XPS, and synthesis mechanism analysis, WO_3NCs@LoP were successfully synthesized with regular morphology and microstructure. Meanwhile, comparing with WO_3NCs, WO_3NCs@LoP had a larger specific surface area, providing more photocatalytic active sites, which was beneficial to the photocatalytic degradation process.

Photochemical properties of WO_3NCs@LoP

In order to explore the optical properties of the WO_3**NCs**, LoP, and WO_3NCs@LoP, UV–Vis diffuse reflectance spectra were conducted because it could verify the absorption of visible light and calculate the band gap energy of the material by Tauc equation. The results were shown in Fig. 5. It could be found that LoP exhibited better visible light absorption ability in the visible light band (400–800 nm), indicating that it utilized visible light energy. However, WO_3NCs had a strong absorption ability in the ultraviolet region, but poor light absorption performance in the visible light region, indicating that it mainly absorbed ultraviolet light. After in situ synthesis of WO_3NCs in LoP via a hydrothermal reaction, the obtained WO_3NCs@LoP showed an enhanced absorption intensity in the visible light region, indicating an obvious red shift. The results manifested that the light absorption range of WO_3NCs was significantly improved

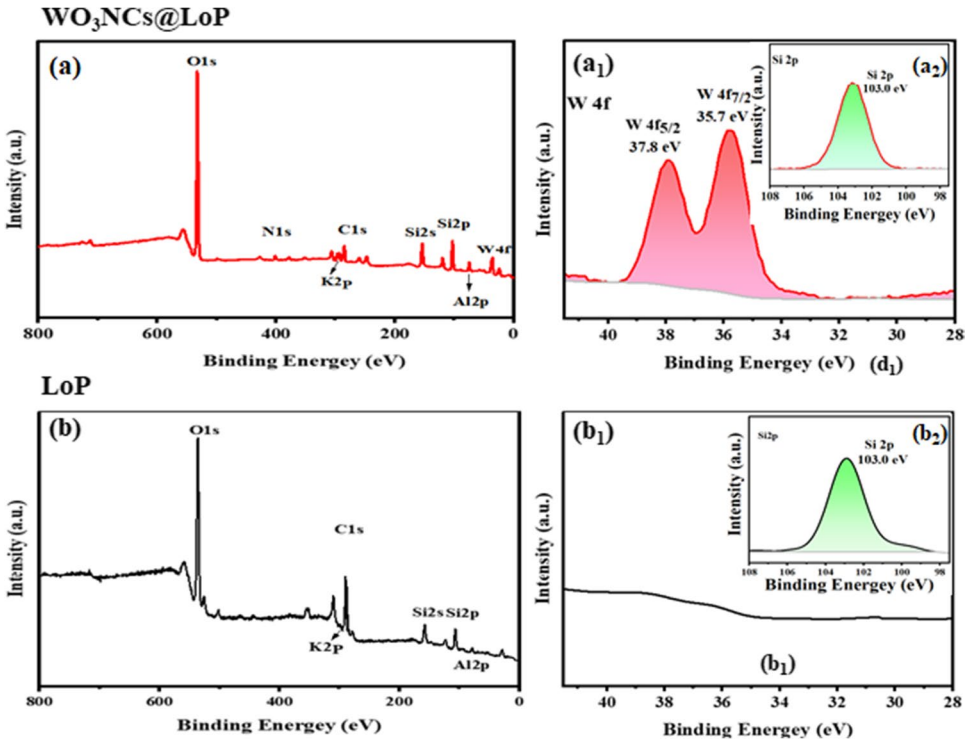

Fig. 4 XPS full spectrum, Si2p, and W4f high resolution spectra of WO_3NCs@LoP (a, a_1, a_2) and LoP (b, b_1, b_2)

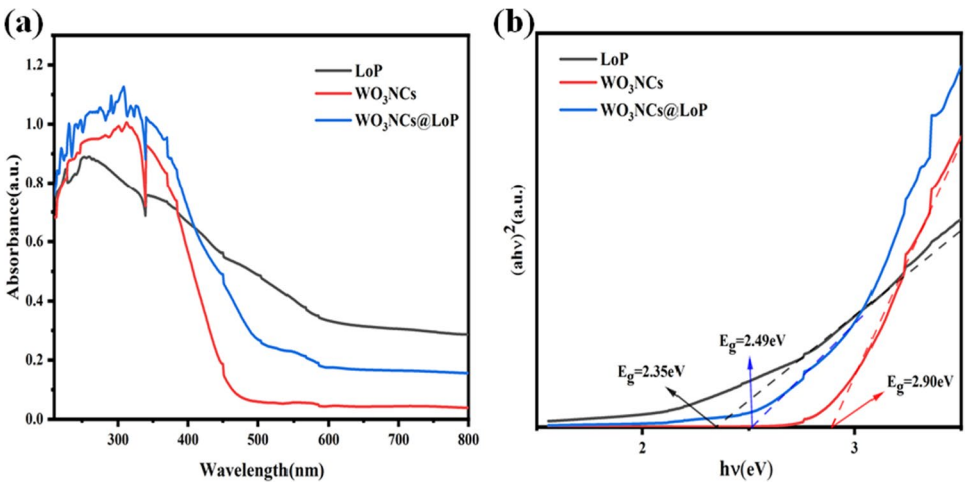

Fig. 5 **a** Diffuse reflectance UV–Vis, **b** band gaps curves of LoP, WO_3NCs, and WO_3NCs@LoP

after the formation of WO_3NCs@LoP. The results showed that the photochemical properties of WO_3NCs could be enhanced by combining WO_3NCs on LoP, separating photogenerated electron–hole pairs occur in WO_3NCs@LoP under visible light.

Furthermore, the band energy (Eg) is calculated by the reported Tauc function in the literature (Xiang et al. 2020): $(\alpha h\nu)^n = A\,(h\nu - Eg)$ where α, $h\nu$, A, Eg, and n indicate the absorption coefficient, Planck constant, photon energy, proportionality constant, energy gap, and the transition properties of semiconductors (indirect semiconductors: $n = 1/2$, direct semiconductors: $n = 2$), respectively (Zhao et al. 2021). Herein, $n = 2$ due to the as-prepared solid samples have direct semiconductor properties. According to the calculation, the band gap of WO_3NCs was 2.90 eV; for the WO_3NCs@LoP, its Eg was 2.49 eV, which were exhibited in Fig. 5b. Of note, WO_3NCs@LoP had narrow band width in contrast with WO_3NCs. As a consequence, WO_3NCs@LoP photocatalyst used visible light to promote more efficient separation of photogenerated electron–hole pairs, which further improved the photocatalytic performance. Moreover, the conduction band potential (CB) and valence band potential (VB) can be calculated via the following formula (Eqs. (3), (4)), where Xis the electronegativity of the semiconductor, E_{VB} is the VB potential, E_{CB} is the CB potential, and Ee is the energy of the e^- in the Hscale (~4.5 eV) (Roy

et al., 2022). According to the above equation, the E_{CB} and E_{VB} values of WO_3NCs and WO_3NCs@LoP were calculated as follows: for WO_3, $E_{CB} = 0.63$ eV and $E_{VB} = 3.53$ eV; for WO_3NCs@LoP, $E_{CB} = 0.845$ eV and $E_{VB} = 3.335$ eV. The results indicated that WO_3NCs@LoP composite materials could greatly enhance optical absorption in visible light due to synergistic effect among WO_3NCs and LoP, which was beneficial to enhance the photocatalytic activity.

$$(\alpha hv)^n = A(hv - Eg) \tag{2}$$

$$E_{CB} = X - E_C - 0.5Eg \tag{3}$$

$$E_{VB} = E_{CB} + Eg \tag{4}$$

Photocatalytic activity

To explore the photocatalytic activity of the prepared photocatalysts, a common ionic dye MB in the textile industry was selected as the degradation substrate. A series of degradation experiments performed were shown in Fig. 6. The effects of photocatalyst dosage, MB concentration, irradiation time, and pH value were explored. Discussion and validation of the effects of experimental conditions on MB degradation experiments were in the Supporting Information (Fig S3–S6). The results denoted that the optimal conditions were photocatalyst 0.05 g, MB 20 mg/L, irradiation time 20 min, and no pH adjustment. Figure 6a shows the degradation curves of MB by different catalysts, and it was found that MB was a relatively stable dye with hardly self-degradation without any catalyst. The removal rate of LoP with the favorable adsorption capacity reached 54.4% after the equilibrium of adsorption and desorption, and the final removal rate reached 62.1%, indicating its poor photodegradation performance. After the adsorption–desorption equilibrium of WO_3NCs, the removal rate was only 29.0%, while the final MB removal rate reached 66.1% under visible light irradiation, indicating that WO_3NCs presented photocatalytic degradation of MB. WO_3NCs@LoP as a photocatalyst photodegrades MB under the same conditions, and it could be observed that the removal rate of MB was higher than that of pure WO_3NCs and LoP, with a final removal rate of 99.8% and an adsorption capacity of 47.9%. It was worth mentioning that the degradation rate of WO_3NCs@LoP reached 99.5% under visible light irradiation for only 20 min and proved that the prepared photocatalyst was an efficient photocatalyst with excellent photocatalytic performance.

To study the catalytic activity of the photocatalysts, a pseudo-first-order kinetic model was used for fitting to compare the degradation rates of MB under different photocatalysts, and the reaction rate constants were shown in Fig. 6b (Dai et al. 2021; Valério et al. 2020). It could be observed that the size of the apparent reaction rate was WO_3NCs@LoP (0.0495 min^{-1}) > WO_3NCs (0.0074 min^{-1}) > LoP (0.0047 min^{-1}). WO_3NCs@LoP showed the highest apparent reaction rate, which was about 10.53 and 6.69 times higher than pure LoP and WO_3NCs,

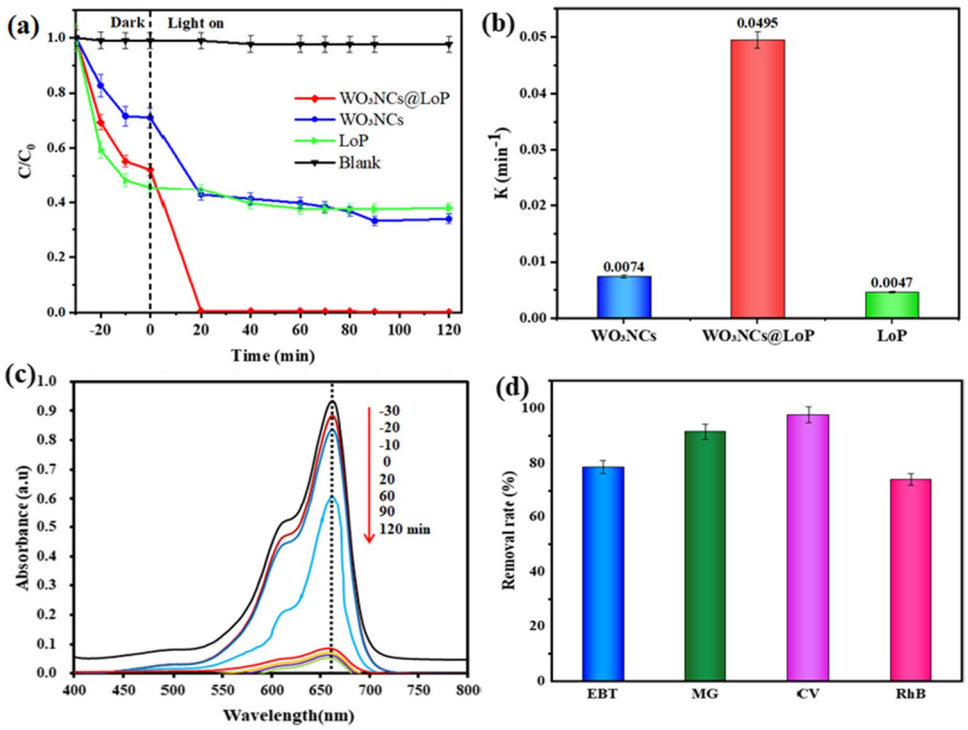

Fig. 6 The degradation curves (**a**) and the pseudo first-order kinetic (**b**) of MB degradation with different photocatalysts, UV–Vis spectra MB solution during photodegradation (**c**), and comparison of photocatalytic degradation of WO_3NCs@LoP by different dyes (**d**)

respectively. In WO_3NCs@LoP, the photocatalytic activity of WO_3NCs was significantly enhanced after WO_3NCs loaded on the LoP surface. The reason was that WO_3NCs uniformly attached on the surface of LoP, which not only improved the agglomeration of WO_3NCs, but also increased the specific surface area of the catalyst, so that the catalyst provided more active sites during the photocatalytic degradation process. At the same time, the synergistic effect of LoP and WO_3NCs enhanced the photocatalytic performance of the catalyst. After being photodegraded by WO_3NCs@LoP, the change of MB concentration under different illumination times was measured by UV–Vis spectroscopy as shown in Fig. 6c, with the maximum absorption peak at 664 nm. With the increase of photocatalytic degradation time, the intensity of the absorption peak obviously gradually weakened, which indicated that the residual MB concentration in the solution gradually decreased.

The lowest value was almost reached at 20 min, which was not much different from the maximum degradation value at 90 min, indicating that MB in the solution was almost completely degraded within 20 min of photodegradation. In another side, near 50 % of dyes were absorbed in darkness from -30 to 0 min. It proved that adsorption played an important role in the degradation process, and it was demonstrated that this process synergistic effect of photocatalytic degradation and adsorption. In general, most photocatalysts were not widely used because they do not possess degradation universality. In this study, the degradation performance of WO_3NCs@LoP for other ionic dyes was investigated, and the results were shown in Fig. 6d. It could be clearly found that WO_3NCs@LoP showed a good degradation effect on EBT, MG, CV, and RhB, and the lowest degradation rate also reached more than 75%, indicating that the material denoted a wide range of dye degradation properties.

It is well known that WO_3NCs is a typical photocatalyst (Shandilya et al. 2022), and several studies denote reported its photocatalytic degradation performance. The degradation performance of the prepared photocatalysts for MB was compared with the reported literatures (Table 1). The results were shown that WO_3NCs@LoP expressed excellent performance in terms of dosage, irradiation time, and final removal rate, indicating that the photocatalyst prepared in this experiment expressed a good degradation effect.

Cycling stability of photocatalytic degradation

The cycling stability of photocatalysts is an important indicator to investigate (Gu et al. 2022). In view of this factor, the cycle stability of the catalyst was investigated, and the results were shown in Fig. 7. The photocatalytic degradation of MB was consistent with the above-mentioned process. The used photocatalyst was collected, washed with

Table 1 Comparison with other WO_3NCs@LoP-based photocatalysts on MB degradation

Photocatalysts	Dosage (mg)	MB (mg/L)	Irradiation time (min)	Removal rate (%)	K value (min^{-1})	Ref
$WO_3/NiWO_4$	20	10.0	80 min	90.63	0.0289	Thilagavathi et al. (2021)
$ZnWO_4/WO_3$	2	5	120 min	83.60	0.013	MohanKumar et al. (2022)
WO_3-CuS	125	5.0	85 min	90.0	—	Liu et al. (2020)
WO_3	50	40	20 min	50.50	—	Zhang et al. (2017)
ZnS-WO_3-$CoFe_2O_4$	50	50	180 min	95.97	0.0138	Palanisamy et al. (2021)
WO_3NCs@LoP	50	20	90 min	99.84	0.0495	This work

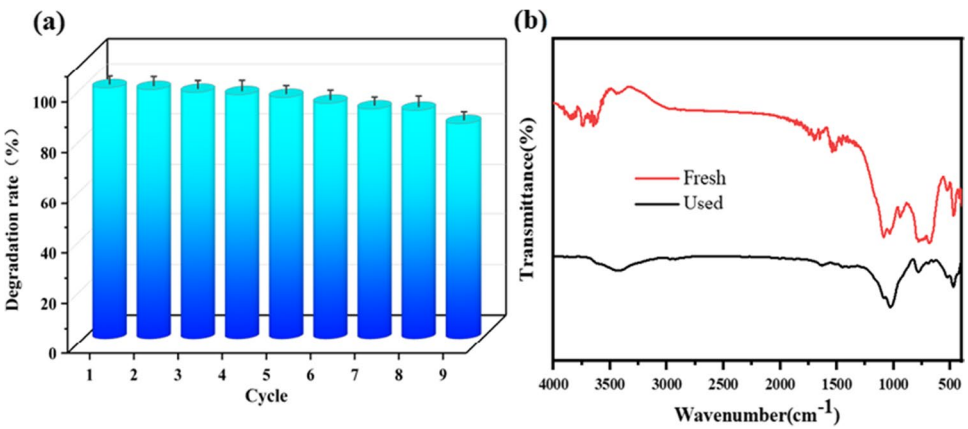

Fig. 7 **a** The catalytic degradation performance after repeated experiments, **b** FT-IR spectra of WO_3NCs@LoP photocatalyst before and after nine experiments

redistilled water and absolute ethanol by centrifugation, and dried, and the recovered catalyst was recycled. The MB degradation rate of WO_3NCs@LoP still reached above 85% after 9 cycles (Fig. 7a). It was proved that WO_3NCs@LoP had excellent photocatalytic activity, which might be related to the tight interface formed by the combination of WO_3NCs and LoP due to the hydrothermal reaction. At the same time, WO_3NCs@LoP also possessed excellent photocatalytic stability. The structure of the photocatalyst (WO_3NCs@LoP) before and after the degradation reaction was characterized by FT-IR (Fig. 7b). It indicated that characteristic peaks of W–O-W bond near 800 ~ 645 cm^{-1} were weakened after cycling, and the characteristic peaks of Si–O-Si bonds still existed, indicating some WO_3NCs were run away after 9 cycles of degradation process. In conclusion, WO_3NCs@LoP is a photocatalyst with excellent photocatalytic activity and stability.

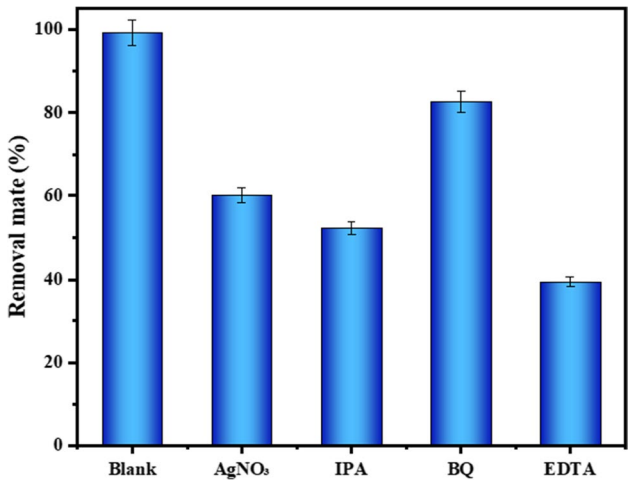

Fig. 8 Active substance capture experiment

Capture of radical experiment

It is well known that active species play an extremely crucial role in the photocatalytic degradation process (Cai et al. 2022). With a view to identifying the active species in the process of degrading MB and providing a strong proof for the degradation mechanism, the capture experiment of active species in the photodegradation process of MB by WO_3NCs@LoP was produced under visible light. The results were shown in Fig. 8; it could be found that with the addition of $AgNO_3$, IPA and EDTA significantly inhibited the MB degradation, while BQ had little effect on the degradation process. Therefore, e^-, h^+, and •OH were the active substances that played a role in the photocatalytic degradation of MB.

Photocatalytic mechanism of WO_3NCs@LoP

On the basis of aforementioned characterization and experimental result analysis, the possible mechanism for high degradation efficiency of WO_3NCs@LoP composites is proposed under visible light, and showed in Scheme 2. When visible light irradiated on the surface of the catalyst, it produced the electron–hole pairs for photocatalytic degradation of MB (Eqs., 5, 6 and 7). Obviously, the higher VB potential of WO_3NCs@LoP (3.33 V vs NHE) than H_2O/•OH (2.13 eV vs NHE) was capable of oxidizing and adsorbing H_2O to produce •OH. Meanwhile, parts of the hole could act as an active substance to degradate MB, whereas the CB accumulated electrons of WO_3NCs@LoP could not reduce O_2 to form $\bullet O_2^-$ owing to the higher CB potential of WO_3NCs@LoP (0.845 V vs NHE) than $O_2/\bullet O_2^-$ (−0.33 eV vs NHE). As a consequence, it was demonstrated that decomposition of hydroxyl radicals (•OH), e^-, and photogenerated holes (h^+) was the more effective active substance in the process of photodegradation, which could directly react

Scheme 2 Photocatalytic mechanism of WO_3NCs@LoP

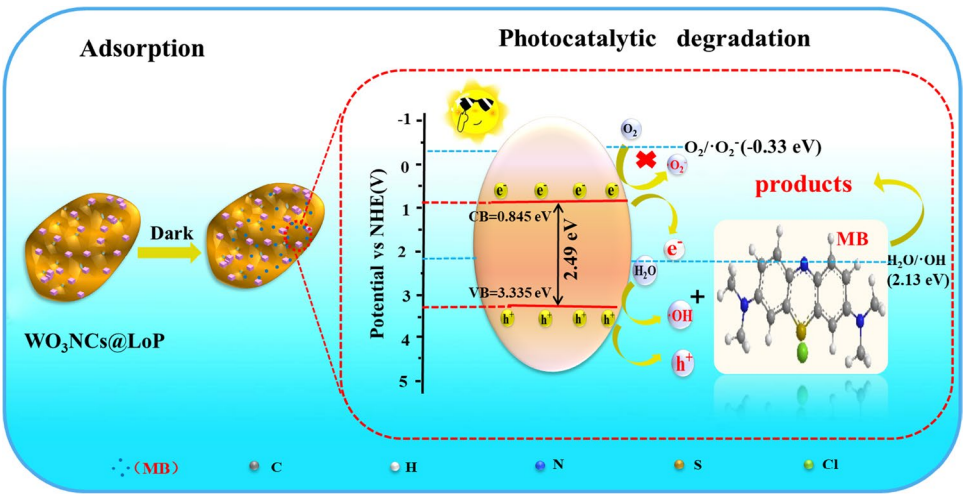

with MB to further oxidize it (Eq. (8)). This was consistent with the results of the active substance capture experiment above. Thus, the significantly improved catalytic activity of WO_3NCs@LoP photocatalyst under visible light could depend on the effective separation mechanism of photogenerated electron–hole pairs.

$$WO_3NC_s \rightarrow WO_3NC_s\left(e^- + h^+\right) \quad (5)$$

$$WO_3NC_s@LoP + hv \rightarrow WO_3NC_s\left(e^- + h^+\right) \quad (6)$$

$$H_2O + h^+ \rightarrow \bullet OH \quad (7)$$

$$\bullet OH + h^+ + e^- + MB \rightarrow Products \quad (8)$$

Conclusions

In summary, a novel WO_3NCs@LoP composite photocatalyst has been triumphantly synthesized by a facile one-pot hydrothermal with the loading of WO_3NCs on LoP, which not only improves the agglomeration of WO_3NCs, but also enhances the photocatalytic activity. The morphologies, functional groups, crystal phase, band gap, composition, and chemical structure were analyzed by SEM, FT-IR, XRD, UV–Vis DRS, and XPS, which demonstrated the successful synthesis of composite material and deep look into the possible mechanism. Under visible light irradiation, compared to the pure WO_3NCs and LoP, WO_3NCs @ LoP composite material exhibited an excellent degradation effect on MB, and the removal rate in 20 min reached more than 99%, with the apparent reaction rate of 0.0495 min^{-1}, which was about 10.53 and 6.69 times higher than pure LoP and WO_3NCs, respectively. At the same times, composite photocatalyst WO_3NCs@LoP demonstrated favorable stability, and the degradation rate of MB remained reach more than 85% after recycling 9 times. A photocatalyst based on the loess substrate presents good performance and low cost; there will have broad application prospects and also respond to environmentally friendly materials for organic pollutions in wastewater treatment.

Supplementary Information The online version contains supplementary material available at https://doi.org/10.1007/s11356-022-21633-9.

Author contribution Hua Yang: Writing, original draft; data curation; formal analysis. Peiyu Cao: Data curation; writing, review and editing; formal analysis; software. Yaping Zhang: Validation, writing—review and editing. Meiling Zhou: Visualization. Yufeng He: Project administration, visualization. Pengfei Song: Visualization. RongminWang: Supervision, project administration, funding acquisition, conceptualization, writing—review and editing. All authors read and contributed to the manuscript.

Funding The project was supported by the National Natural Science Foundation of China (21865030).

Data availability All data generated or analyzed during this study are included in this published article [and its supplementary information files.

Declarations

Ethics approval and consent to participate Not applicable.

Consent for publication Not applicable.

Competing interests The authors declare no competing interests.

References

Abdelmaksoud M, Mohamed A, Sayed A, Khairy S (2021) Physical properties of PVDF-GO/black-TiO_2 nanofibers and its photocatalytic degradation of methylene blue and malachite green dyes. Environ Sci Pollut Res 28:30613–30625. https://doi.org/10.1007/s11356-021-12618-1

Ahmadi SAR, Kalaee MR, Moradi O, Nosratinia F, Abdouss M (2022) Synthesis of novel zeolitic imidazolate framework (ZIF-67) – zinc oxide (ZnO) nanocomposite (ZnO@ZIF-67) and potential adsorption of pharmaceutical (tetracycline (TCC)) from water. J Mol Struct 1251:132013. https://doi.org/10.1016/j.molstruc.2021.132013

Ahmadi SAR, Kalaee MR, Moradi O, Nosratinia F, Abdouss M (2021) Core–shell activated carbon-ZIF-8 nanomaterials for the removal of tetracycline from polluted aqueous solution. Adv Compos Mater 4:1384–1397. https://doi.org/10.1007/s42114-021-00357-3

Al-Kuhailia MF, Drmoshb QA (2022) Investigating the structural and optoelectronic properties of co-sputtered Fe-doped WO_3 thin films and their suitability for photocatalytic applications. Mater Chem Phys 281:125897. https://doi.org/10.1016/j.matchemphys.2022.125897

Babaei M, Azar PA, Tehrani MS, Farjaminezhad M, Hussain SW (2022) Green and simple synthesized graphene/MnO_2 quantum dot nanocomposite: characterization and application as an efficient adsorbent for solid-phase extraction of heavy metals. J Nanostructure Chem 12:249–261. https://doi.org/10.1007/s40097-021-00410-z

Babudurai M, Nwakanma O, Romero-Nuñez A, Manisekaran R, Subramaniam V, Castaneda H, Jantrania A (2021) Mechanical activation of TiO_2/Fe_2O_3 nanocomposite for arsenic adsorption: effect of ball-to-powder ratio and milling time. J Nanostructure Chem 11:619–632. https://doi.org/10.1007/s40097-021-00388-8

Cai PC, Zhao J, Zhang XH, Zhang TY, Yin GM, Chen S, Dong CL, HuangHC Y-C, Sun YY, Yang DJ, Xing BS (2022) Synergy between cobalt and nickel on $NiCo_2O_4$ nanosheets promotes peroxymonosulfate activation for efficient norfloxacin degradation. Appl Catal B 306:121091. https://doi.org/10.1016/j.apcatb.2022.121091

Cao PY, Zhang YP, Gao D, Chen HX, Zhou ML, He YF, Song PF, Wang RM (2022) Constructing nano-heterojunction of MOFs with crystal regrowth for efficient degradation of tetracycline under visible light. J Alloys Compd 904:164061. https://doi.org/10.1016/j.jallcom.2022.164061

Chen P, Gou YJ, Ni JM, Liang YM, Bingqiao Yang BQ, Jia FF, Song SX (2020) Efficient ofloxacin degradation with Co(II)-doped MoS_2 nano-flowers as PMS activator under visible-light

irradiation. Chem Eng J 401:125978. https://doi.org/10.1016/j.cej.2020.125978
Cheng PP, Jin Q (2022) Performance evaluation of the emerging rural sewage treatment facilities in China. Environ Sci Pollut Res. https://doi.org/10.1007/s11356-022-19467-6
Cui XF, Zhou Y, Wu J, Ling S, Zhao LJ, Zhang JL, Wang JW, Qin W, Zhang YG (2020) Controlling Pt co-catalyst loading in a WO_3 quantum dot and MoS_2 nanosheet composite Z-scheme system for enhanced photocatalytic H_2 evolution. Nanotechnol 31:185701. https://doi.org/10.1088/1361-6528/ab6ab3
Dai DL, Qiu JH, Li M, Xu J, Zhang L, Yao JF (2021) Construction of two-dimensional BiOI on carboxyl-rich MIL-121 for visible-light photocatalytic degradation of tetracycline. J Alloy Compd 872:159711. https://doi.org/10.1016/j.jallcom.2021.159711
Deng XR, Jiang YF, Zhang M, Nan ZJ, Liang XR, Wang G (2022) Sorption properties and mechanisms of erythromycin and ampicillin in loess soil: roles of pH, ionic strength, and temperature. Chem Eng J 434:134694. https://doi.org/10.1016/j.cej.2022.134694
Dhanalakshmi M, Lakshmi Prabavathi S, Saravanakumar K, Filip Jones B, Muthuraj V (2020) Iridium nanoparticles anchored WO_3 nanocubes as an efficient photocatalyst for removal of refractory contaminants (crystal violet and methylene blue). Chem Phys Lett 745:137285. https://doi.org/10.1016/j.cplett.2020.137285
Gao CY, Xu L, Coop MR, Huang C, Zuo L (2021) An investigation of particle breakage in loess. Bull Eng Geol Environ 286:106083. https://doi.org/10.1016/j.enggeo.2021.106083
Gu JB, Li QW, Long XY, Zhou XH, Liu N, Li ZQ (2022) Fabrication of magnetic dual Z-scheme heterojunction materials for efficient photocatalytic performance: the study of ternary novel MIL-88A(Fe)/BiOBr/$SrFe_{12}O_{19}$ nanocomposite. Sep Purif Technol. https://doi.org/10.1016/j.seppur.2022.120778
Guo H, Jiang N, Wang HJ, Shang KF, Lu N, Li J, Wu Y (2019) Pulsed discharge plasma induced WO_3 catalysis for synergetic degradation of ciprofloxacin in water: synergetic mechanism and degradation pathway. Chemosphere 230:190–200. https://doi.org/10.1016/j.chemosphere.2019.05.011
Gupta VK, Moradi O, Tyagi I, Agarwal S, Sadegh H, Shahryari-Ghoshekandi R (2015) Study on the removal of heavy metal ions from industry waste by carbon nanotubes: effect of the surface modification: a review. Crit Rev Environ Sci Technol 46:93–118. https://doi.org/10.1080/10643389.2015.1061874
Kamaludin R, Othman MHD, Kadir SH, Ismail AF, Rahman MA (2018) Visible-light-driven photocatalytic N-doped TiO_2 for degradation of bisphenol A (BPA) and reactive Black 5 (RB5) dye. Water Air Soil Pollut 229(11):363. https://doi.org/10.1007/s11270-018-4006-8
Karami MH, Kalaee M, Khajavi R, Moradi O, Zaarei D (2022) Thermal degradation kinetics of epoxy resin modified with elastomeric nanoparticles. Adv Compos Mater 5:390–401. https://doi.org/10.1007/s42114-022-00419-0
Li Y, Yeung KL (2019) Polymeric catalytic membrane for ozone treatment of DEET in water. Catal Today 331:53–59. https://doi.org/10.1016/j.cattod.2018.06.005
Li YC, Yu B, Hu ZQ, Wang H (2022) Construction of direct Z-scheme SnS_2@$ZnIn_2S_4$@kaolinite heterostructure photocatalyst for efficient photocatalytic degradation of tetracycline hydrochloride. Chem Eng J 429:132105. https://doi.org/10.1016/j.cej.2021.132105
Liu H, Zhang Y, Yang J, Wang H, Li Y, Shi Y, Li D, Holm PE, Ou Q, Hu W (2021) Quantitative source apportionment, risk assessment and distribution of heavy metals in agricultural soils from southern Shandong Peninsula of China. Sci Total Environ 767:144879. https://doi.org/10.1016/j.scitotenv.2020.144879
Liu Y, Wang G, Yang W, Yang J, Li J (2019) Biotemplated synthesis of hierarchically porous ZnAl-CLDH/$FeWO_4$ for effective removal of dyes from water. Water Air Soil Pollut 230(4):89. https://doi.org/10.1007/s11270-019-4134-9
Liu YT, Li M, Zhang QY, Qin PC, Wang XD, He GN, Li L (2020) One-step synthesis of a WO_3-CuS nanosheet heterojunction with enhanced photocatalytic performance for methylene blue degradation and Cr(VI) reduction. J Chem Technol Biotechnol 95:665–674. https://doi.org/10.1002/jctb.6247
Lu QB, Wang Y, Zhang D, Cong HL (2022) Solar light-driven photocatalytic production of hypochlorous acid over Pt/WO_3 in seawater for marine antifouling. Res Chem Intermed 48:29–47
Malinga NN, Jarvis ALL (2020) Synthesis, characterization and magnetic properties of Ni, Co and FeCo nanoparticles on reduced graphene oxide for removal of Cr(VI). J Nanostructure Chem 10:55–68. https://doi.org/10.1007/s40097-019-00328-7
Manikandan VS, Harish S, Archana J, Navaneethan M (2022) Fabrication of novel hybrid Z-Scheme WO_3 @g-C_3N_4 @MWCNT nanostructure for photocatalytic degradation of tetracycline and the evaluation of antimicrobial activity Chemical Society Reviews. Chemosphere 287:132050. https://doi.org/10.1016/j.chemosphere.2021.132050
Masocha BL, Dikinya O, Moseki B (2022) Bioavailability and contamination levels of Zn, Pb, and Cd in sandy-loam soils. Botswana Environ Earth Sci 81:171. https://doi.org/10.1007/s12665-021-10129-3
Mehmood F, Iqbal J, Ismail M, Mehmood A (2018) Ni doped WO_3 nanoplates: an excellent photocatalyst and novel nanomaterial for enhanced anticancer activities. J Alloys Compd 746:729–738. https://doi.org/10.1016/j.jallcom.2018.01.409
Mirzaeian MM, Eskandari L, Rashidi AM (2019) Synthesis of graphene oxide-supported meso-tetrakis (4-carboxyphenyl) porphyrinatoiron (III) chloride as a heterogeneous nanocatalyst for the mercaptan removal from the gas stream. J Nanostructure Chem 9:19–28. https://doi.org/10.1007/s40097-019-0294-9
MohanKumar G, Lee DJ, Jeon HC, Ilanchezhiyan P, Young KD, Won KT (2022) One dimensional $ZnWO_4$ nanorods coupled with WO_3 nanoplates heterojunction composite for efficient photocatalytic and photoelectrochemical activity. Ceram Int 48:4332–4340. https://doi.org/10.1016/j.ceramint.2021.10.228
Moradi O, Aghaie M, Zare K, Monajjemi M, Aghaie H (2009) The study of adsorption characteristics Cu^{2+} and Pb^{2+} ions onto PHEMA and P(MMA-HEMA) surfaces from aqueous single solution. J Hazard Mater 170:673–679. https://doi.org/10.1016/j.jhazmat.2009.05.012
Moradi O, Madanpisheh MA, Moghaddas M (2021) Synthesis of GO/HEMA, GO/HEMA/TiO_2, and GO/Fe_3O_4/HEMA as novel nanocomposites and their dye removal ability. Adv Compos Mater 4:1185–1204. https://doi.org/10.1007/s42114-021-00353-7
Moradi O, Sharma G (2021) Emerging novel polymeric adsorbents for removing dyes from wastewater: a comprehensive review and comparison with other adsorbents. Environ Res 201:111534. https://doi.org/10.1016/j.envres.2021.111534
Mukhtar F, Munawar T, Nadeem MS, Rehman MN, Batool S, Hasan M, Riaz M, Rehman K, Iqbal F (2021) Highly efficient tri-phase TiO_2–Y_2O_3–V_2O_5 nanocomposite: structural, optical, photocatalyst, and antibacterial studies. J Nanostructure Chem. https://doi.org/10.1007/s40097-021-00430-9
Naeimi A, Sharifi AK, Montazerghaem L, Abhari AR, Mahmoodi Z, Zinab H, Bakr AV, Soldatov GAM (2022) Transition metals doped WO_3 photocatalyst towards high efficiency decolourization of azo dye. J Mol Biol 1250:131800. https://doi.org/10.1016/j.molstruc.2021.131800
Naeini AH, Kalaee MR, Moradi O, Khajavi R, Abdouss M (2022) Synthesis, characterization and application of carboxylmethyl cellulose, Guar gam, and graphene oxide as novel composite adsorbents for removal of malachite green from aqueous

solution. Adv Compos Mater 5:335–349. https://doi.org/10.1007/s42114-021-00388-w

Ouyang C, Quan XY, Zhang CL, Pan YX, Li XY, Hong ZL, Zhi MJ (2021) Direct Z-scheme $ZnIn_2S_4$@MoO_3 heterojunction for efficient photodegradation of tetracycline hydrochloride under visible light irradiation. Chem Eng J 424:130510. https://doi.org/10.1016/j.cej.2021.130510

Palanisamy G, Bhuvaneswari K, Bharathi G, Pazhanivel T, Andrews SK, Pasha K (2021) Construction of magnetically recoverable ZnS–WO_3–$CoFe_2O_4$ nanohybrid enriched photocatalyst for the degradation of MB dye under visible light irradiation. Chemosphere 273:129687. https://doi.org/10.1016/j.chemosphere.2021.129687

Parthibavarman M, Karthik M, Prabhakaran S (2018) Facile and one step synthesis of WO_3 nanorods and nanosheets as an efficient photocatalyst and humidity sensing material. Vacuum 155:224–232. https://doi.org/10.1016/j.vacuum.2018.06.021

Raeisi I, Derakhshi P, Azar PA, Tehrani MS (2021) Desulfurization of gas condensate under visible light using synthesized photocatalysts of Mn/TiO_2/MWCNTs and Ni/TiO_2/MWCNTs. J Nanostructure Chem 11:165–185. https://doi.org/10.1007/s40097-020-00349-7

Rajabi M, Mahanpoora K, Moradi O (2019) Preparation of PMMA/GO and PMMA/GO-Fe_3O_4 nanocomposites for malachite green dye adsorption: kinetic and thermodynamic studies. Compos B Eng 167:544–555. https://doi.org/10.1016/j.compositesb.2019.03.030

Rajabi M, Mahanpoora K, Moradi O (2017) Removal of dye molecules from aqueous solution by carbon nanotubes and carbon nanotube functional groups: critical review. RSC Adv 7:47083–47090. https://doi.org/10.1039/C7RA09377B

Rajendran K, Shanmugasundaram M, Arulanandhu DM, Gopu G, Kalaignan GP, Jeon B, Subbaiah MP (2021) Oxalic acid-induced assembly of CoxNi1−x-bimetallic polyaniline nanocomposite: a bifunctional material for supercapacitor and chromium removal applications. J Nanostructure Chem. https://doi.org/10.1007/s40097-021-00425-6

Robati D, Mirza B, Rajabi M, Moradi O, Tyagi I, Agarwal S, Gupta VK (2016) Removal of hazardous dyes-BR 12 and methyl orange using graphene oxide as an adsorbent from aqueous phase. Chem Eng J 284:687–697. https://doi.org/10.1016/j.cej.2015.08.131

Roy D, Neogi S, De S (2022) Mechanistic investigation of photocatalytic degradation of bisphenol-A using MIL-88A(Fe)/MoS_2 Z-scheme heterojnction composite assisted peroxymonosulfate activation. Chem Eng J 428:131028. https://doi.org/10.1016/j.cej.2021.131028

Shah JH, Fiaz M, Athar M, Ali J, Rubab M, Mehmood R, Jamil SUU, Djellabi R (2020) Facile synthesis of n/b-double-doped Mn_2O_3 and WO_3 nanoparticles for dye degradation under visible light. Environ Sci Technol 41(18):2372–2381. https://doi.org/10.1080/09593330.2019.1567604

Shandilya P, Sambyal S, Sharma R, Mandyal P, Fang BZ (2022) Properties, optimized morphologies, and advanced strategies for photocatalytic applications of WO_3 based photocatalysts. J Hazard Mater 428:128218. https://doi.org/10.1016/j.jhazmat.2022.128218

Shen Y, Yan HY, Song PF, He YF, Wang RM (2021) Progress with functional materials based on loess particles. Clays Clay Miner 69:301–314. https://doi.org/10.1007/s42860-021-00123-y

Shi W, Li T, Yan Feng SuH, Yang Q (2022) Source apportionment and risk assessment for available occurrence forms of heavy metals in Dongdahe Wetland sediments, southwest of China. Sci Total Environ 815:152837. https://doi.org/10.1016/j.scitotenv.2020.140310

Shi ZL, Wang YM, Sun SY, Zhang C, Wang HB (2020) Removal of methylene blue from aqueous solution using Mg-Fe, Zn-Fe, Mn-Fe layered double hydroxide. Water Sci Technol 81(12):2522–2532. https://doi.org/10.2166/wst.2020.313

Sun JY, Li BH, Wang Q, Zhang P, Zhang YL, Li G, Li XC (2020) Preparation of phosphorus-doped tungsten trioxide nanomaterials and their photocatalytic performances. Environ Technol. https://doi.org/10.1080/09593330.2020.1745292

Sun L, Li LL, Fan JJ, Xu QL, Ma DK (2022) Construction of highly active WO_3/TpPa-1-COF S-scheme heterojunction toward photocatalytic H_2 generation. J Mater Sci Technol. https://doi.org/10.1016/j.jmst.2021.12.065

Tahir MB, Rafique M, Isa KM, Majid A, Nazar F, Sagir M, Gilani S, Farooq M, Ahmed A (2018) Enhanced photocatalytic hydrogen energy production of g-C_3N_4-WO_3 composites under visible light irradiation. Int J Energy Res 42(15):4667–4673. https://doi.org/10.1002/er.4208

Thilagavathi T, Venugopal D, Thangaraju D, Marnadu R, Palanivel B, Imran M, Shkir M, Ubaidullah M, AlFaify S (2021) A facile co-precipitation synthesis of novel WO_3/$NiWO_4$ nanocomposite with improved photocatalytic activity. Mater Sci Semicond Process 133:105970. https://doi.org/10.1016/j.mssp.2021.105970

Truong H, Bae S, Cho J, Hur J (2022) Advances in application of g–C_3N_4–based materials for treatment of polluted water and wastewater via activation of oxidants and photoelectrocatalysis. Chemosphere 286:131737. https://doi.org/10.1016/j.chemosphere.2021.131737

Valério A, Wang J, Tong S, Antonio A, Souza D, González HS (2020) Synergetic effect of photocatalysis and ozonation for enhanced tetracycline degradation using highly macroporous photocatalytic supports. Chem Eng Process 149:107838. https://doi.org/10.1016/j.cep.2020.107838

Xiang H, Ren G, Yang X, Xu D, Zhang Z, Wang X (2020) A low-cost solvent-free method to synthesize α-Fe_2O_3 nanoparticles with applications to degrade methyl orange in photo-fenton system. Ecotoxicol Environ Saf 200:110744. https://doi.org/10.1016/j.ecoenv.2020.110744

Xu XY, Zhou JH, Chen K, Wang Y, Ai YM, Zhang CY, Zhou SB (2022) Effect of indole-3-acetic acid supplementation on the physiology of Lolium perenne L. and microbial activity in cadmium-contaminated soil. Environ Sci Pollut Res. https://doi.org/10.1007/s11356-022-19417-2

Ye Z, Zhou ZH, Zhang Y, Zhao LF, Zeng YW (2022) Fe^{3+}-assistantly carbon-impregnated porous SiO_2 mesoscale tubes as Li-ion battery anode materials with highly enhanced performances. Int J Hydrog Energy 47:13442–13459. https://doi.org/10.1016/j.ijhydene.2022.02.085

Zhang N, Li F, Yin YY, Han J, Li X, Liu CX, Zhou JR, Wen SP, Adimi S, Chen Y, Song X, Ruan SP (2021) Gas sensor based on TiO_2 nanofibers decorated with monodispersed WO_3 nanocubes for fast and selective xylene detection. Mater Sci Eng 263:114901. https://doi.org/10.1016/j.mseb.2020.114901

Zhang SY, Li H, Yang ZF (2017) Controllable synthesis of WO_3 with different crystalline phases and its applications on methylene blue removal from aqueous solution. J Alloys Compd 722:555–563. https://doi.org/10.1016/j.jallcom.2017.06.095

Zhao W, Li YJ, Zhao PS, Zhang LL, Dai BL, Huang HB, Zhou JL, Zhu YK, Ma KR, Leung DYC (2021) Insights into the photocatalysis mechanism of the novel 2D/3D Z-Scheme g-C_3N_4/SnS_2 heterojunction photocatalysts with excellent photocatalytic performances. J Hazard Mater 402:123711–1123425. https://doi.org/10.1016/j.jhazmat.2020.123711